Steered molecular dynamics studies reveal different unfolding pathways of prions from mammalian and non-mammalian species†

Matteo Pappalardo,[a] Danilo Milardi,[b] Domenico Grasso[a] and Carmelo La Rosa*[a]

Received (in Montpellier, France) 17th January 2007, Accepted 8th March 2007
First published as an Advance Article on the web 28th March 2007
DOI: 10.1039/b700764g

Prion diseases are associated with an abnormal conformational transition involving the prion protein and are known to affect mammals. Here, the different mechanical behaviour of two mammalian, human (HuPrP) and Syrian hamster (ShaPrP), and two non-mammalian, chicken (ChPrP) and turtle (TuPrP), prions was assessed by steered molecular dynamics simulations performed on the globular domains of the four proteins. In mammalian prions a greater resistance to external stretching forces and an earlier occurrence of irreversible events were observed. The different unfolding profile of mammalian prions, ascribable to the intramolecular interactions involving helix 1 with helix 3, implicate the existence of metastable non-native states which may prompt abnormal pathways of protein misfolding and aggregation.

Introduction

Prion diseases are neurodegenerative disorders, which include Creutzfeldt–Jakob disease in humans, and transmissible spongiform encephalopathy (TSE) in cattle. According to the *protein only* hypothesis the disease is caused by an abnormal form of the prion protein PrP,[1] which accumulates in plaques in the brain.[2] This disease-associated form of PrP (PrP^{Sc}) differs from the normal form (PrP^{C}) only in its three-dimensional structure,[3] characterized by an increased β-sheet content as indicated by FTIR and CD experiments.[4] NMR structures of all prion proteins so far obtained have revealed that the whole N-terminal segment is unstructured and that only the C-terminal part possesses a defined three-dimensional structure. For all species of PrP, the structured part consists of three α-helices and a small two-stranded β-sheet. If one bears in mind that TSEs have been documented only for mammalian species, the differences between mammalian and non-mammalian prions should help to shed light on the molecular mechanism underlying the $PrP^{c} \rightarrow PrP^{sc}$ conversion. In order to map this "misfolding" reaction we need to characterize all the intermediate states along the pathway linking the native PrP^{c} to the PrP^{Sc} state. In this light, molecular dynamics (MD) is an effective tool, allowing all of the interactions between protein atoms to be monitored in detail. Because of limitations on simulation times, and height of energy barriers to conformational transitions in proteins, a number of methods have been proposed to accelerate such transitions by the introduction of an external perturbation. In particular, steered molecular dynamics (SMD) techniques have enabled the characterization of protein unfolding using mechanical forces.[5] This method is expected to provide complementary information on the unfolding–misfolding pathways of a protein to that obtainable from bulk chemical and biophysical measurements. In particular, recent works have evidenced that the mechanical properties of proteins may be correlated with their stability.[6]

Here, SMD techniques have been employed to investigate the mechanical stability of the globular C-terminal domain of two mammalian (human and Syrian hamster) and two non-mammalian (chicken and turtle) PrP proteins with the aim of evaluating different behaviours which discriminate the two families of prions. A comparison of the SMD simulations of the four proteins (HuPrP, ShaPrP, ChPrP and TuPrP) evidenced that the two families of prions, mammalian and non-mammalian, behave differently, suggesting a possible relationship between the unfolding mechanism and prion pathogenesis.

Computational details

SMD simulations were carried out using the software NAMD,[7] and the CHARMM 22 force field. The simulations for both mammalian and non-mammalian prion proteins started from the experimentally determined NMR structures of the C-terminal globular domains: human (PDB code 1HJM†), chicken (PDB code 1U3M†), Syrian hamster (PDB code 1B10†) and turtle (PDB code 1U5L†).[8,9] The alignments of sequences from the four prions are reported in Fig. 1. Despite the fact that the sequences of mammalian and non-mammalian prions share only 40% homology, all the investigated structures showed the same global fold.[9] All the structures were first solvated with water using the TIP3 solvent model.[10] The final water box was large enough to contain all protein atoms at the end of unfolding. The size of the water box was 60 × 60 × 150 Å, with about 150 000 water molecules. The solvated molecules were energy-minimized (conjugate gradient) and gradually heated up to 300 K; then they were equilibrated with a 300 K thermal bath for 400 ps. All SMD simulations were carried out by fixing the N atom of the N terminus "fixed atom" and applying an external force to the C

[a] *Dipartimento di Scienze Chimiche, Universita' di Catania, Viale A. Doria 6, 95125 Catania, Italy. E-mail: clarosa@unict.it.; Fax: +39 95 580138; Tel: +39 95 7385114*
[b] *Istituto di Biostrutture e Bioimmagini CNR-Sezione di Catania, Viale A. Doria 6, 95125 Catania, Italy*

† Electronic supplementary information (ESI) available: Links to FirstGlance to view structures corresponding to PDB numbers. See DOI: 10.1039/b700764g

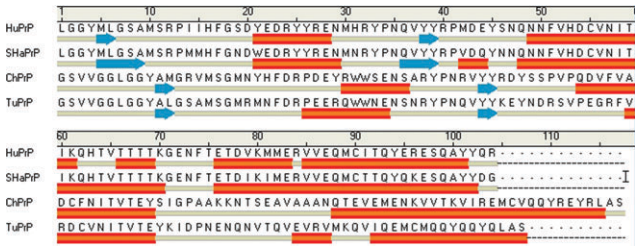

Fig. 1 Alignment of the sequences relative to the globular domains of the four analyzed prion proteins: HuPrP125–228, ShaPrP125–228, ChPrP126–242 and TuPrP119–225. Secondary structure elements such as β-sheets and α-helices are identified as blue arrows and orange bars, respectively.

atom of the C terminus "SMD atom". The direction of elongation was chosen as the vector connecting the fixed atom to the SMD atom. To obtain readable force–elongation profiles it is necessary to connect the SMD atom to a properly chosen virtual spring whose external tip is pulled away along the chosen direction of elongation. The value of the elastic constant K of this spring is a critical parameter and has to be chosen to obtain the best results with an acceptable computational demand. In order to optimize SMD parameters, we have carried out several preliminary trials, all confirming that the best sensitivity for the method could be obtained with a spring constant $K = 10$ kcal mol^{-1} A^{-2} in agreement with other previous papers.[5] A constant pulling rate of 0.1 Å ps^{-1} was chosen to properly balance computational cost and accuracy of simulation. This pulling rate is believed to produce reliable results according to the most commonly adopted simulation protocols.[11] Timestep was fixed at 2 ps, and the "rigid bond" algorithm of NAMD was adopted. Non-bond interactions were treated by adopting a cut-off value of 12 Å. All SMD simulation were performed ten times in order to evaluate statistical fluctuation of the simulations. Only those molecular events that occurred at least 7 times out of 10 simulations were considered meaningful and discussed. In order to evaluate up to what extent the stretching of the proteins can be considered reversible, or in other words, the maximal elongation at with each protein is still capable of refolding, a series of backward simulations were performed starting at increasing extensions (5, 10, 15, 20 and 30 Å) and applying a negative force (not shown). The pulling was considered reversible if consequently to the backward simulation the protein refolded to the native state. All calculations were performed on a Linux cluster of 32 Intel Pentium IV processors. In this configuration, 360 h of CPU time were needed to perform 1 ns of simulation.

Results

All the SMD simulations for the four species, whose force–elongation curves are reported in Fig. 2, started with an equilibrated folded structure and were stopped at an extension of 100 Å, after 1000 ps of simulation. The four proteins exhibit a different unfolding resistance to external forces. This different behaviour originates from these early stages of unfolding and it was not necessary to completely unfold the structures up to a fully extended conformation. Consequently, the force–

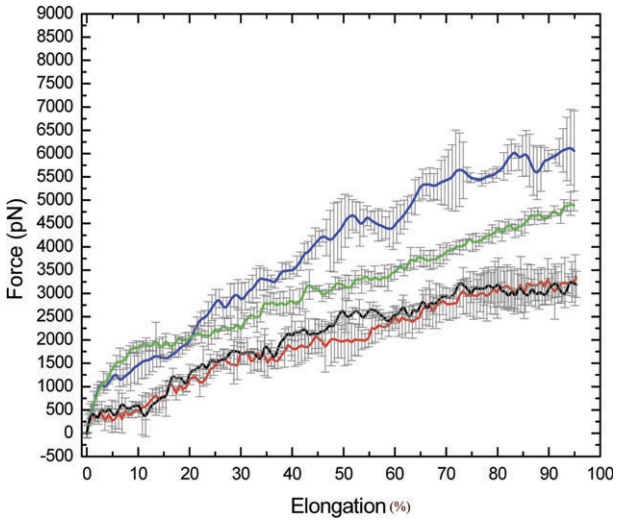

Fig. 2 Force–elongation diagrams obtained from the SMD simulations of the four prion proteins: ShaPrP (blue), HuPrP (green), ChPrP (red) and TuPrP (black). Every solid line represents the mean curve calculated over ten SMD simulations. The bars represent the statistical fluctuation for the simulations.

elongation curves are not biased by the rupture of the intramolecular disulfide bridge connecting helix 2 with helix 3, which is still unbroken at the end of each simulation. Each peak of the four force–elongation curves is ascribable to a particular molecular event involving the loss of native-like contacts, the rupture of a hydrogen bond network or the unfolding of helical structures.

Unfolding of ShaPrP

The unfolding process of ShaPrP can be divided into two regions: in the first, protein stretching is reversible; in the second region, characterized by an irreversible elongation, some structured domains collapse and the protein starts to unfold. This is evidenced in Fig. 3 where some snapshots representing the structure of ShaPrP at different elongations are reported. During the reversible phase (up to 10 Å of elongation), ShaPrP maintains its global fold and the unfolding force never exceeds 1500 pN (see Fig. 2 green line).

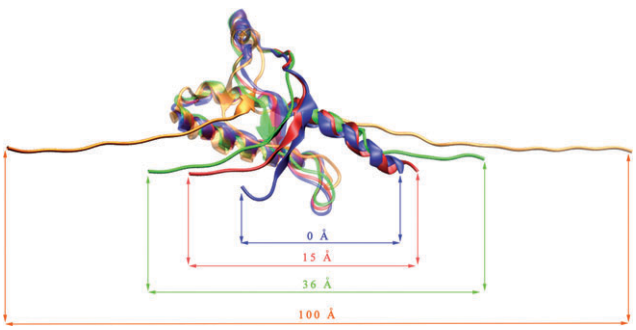

Fig. 3 Ribbon representations of the native (blue), 15 Å-elongated (red), 36 Å-elongated (green) and 100 Å-elongated (yellow) globular domain of ShaPrP. Groups affected by elongation are represented as opaque material. Unmodified regions are represented as transparent material.

Furthermore, the N-terminus, encompassing residues from Leu125 to Met129, unravels evidencing some slight changes in many native-like contacts. After the reversible stretching, an abrupt change in the slope of the force–elongation curve is observed, suggesting that an elongation of 10 Å produces a metastable state which is not able to refold. These changes are better evidenced by looking at the contact maps reported in Fig. 4. In these contact maps, each single spot represents an interaction between two residues—reported in the *x*- and *y*-axes—occurring at less than 7 Å. As discussed before, we reported only the interactions that occurred at least 7 times out of 10 SMD simulations. A comparison of the contact maps evidences that, at the end of the reversible pulling, the native-like contacts of the residues encompassing the last pitch of helix 3 are lost and the interaction existing between Leu130 and Thr216 vanishes. In the meantime, the N-terminal region moves away from helix 3. After this stage of unfolding, in the elongation range 20–30 Å, the helix 3 begins to unfold; here, the unfolding resistance under the unfolding force can be partially attributed to the breaking of a network of hydrogen bonds (H-bonds) involving residues from Ser222 up to Gln227. In the region from 30 to 60 Å, helix 3 continues to unfold and to move away from the protein core. Moreover, the H-bonds connecting the two β-strands involving residues from Met129 to Ala133 and from Gln160 to Tyr163 are broken and the two β-strands slide over each other. In the region from 60 to 66 Å, the two β-strands continue to slide over each other. Here, the H-bonding network connecting the two β-strands is missing, and only weak interactions resist the external pulling force. After an extension of 66 Å, the domain of helix 3 involving residues from Gln212 to Glu219 begins to unfold. At the end of the SMD simulation the force is approximately 6000 pN.

Unfolding of HuPrP

In the region in which the protein exhibits a reversible stretching (0–10 Å), the force rises linearly up to 1500 pN and a number of phenomena occur simultaneously (see Fig. 2 blue line). At first, the C-terminal region of helix 3 starts to unfold and, as evidenced in the contact maps of Fig. 4, several native-like contacts are lost: Met206–Tyr157, Met205–Tyr145, Met205–Tyr149, Val210–Pro158, Val210–Gln160, Cys214–Gln160, Glu221–Met165, Ser222–Met165, Ile215–Asp178, Ile215–Asn171 and Tyr218–Asn17. Differently from the ShaPrP, the N-terminus is almost unmodified. Beyond an extension of 10 Å, the slope of the force–elongation curve changes noticeably, and the stretched protein is not able to refold. Then, four events evidenced at about 33, 50, 64 and 81 Å occur, as shown in Fig. 2. The event located at an extension of 33 Å can be ascribed to the lengthening of helix 3. After an extension of 50 Å, the unfolding of helix 3 begins to appear significant, mainly involving its N-terminal. In addition, the residue Val210 belonging to helix 3 moves away from its original position close to Val180; after this movement the position of helix 3 is tilted. After an extension of 81 Å, the helix 3 unfolds completely and helix 2 begins to bend. At the maximum extension of 100 Å, the unfolding force is about 4500 pN.

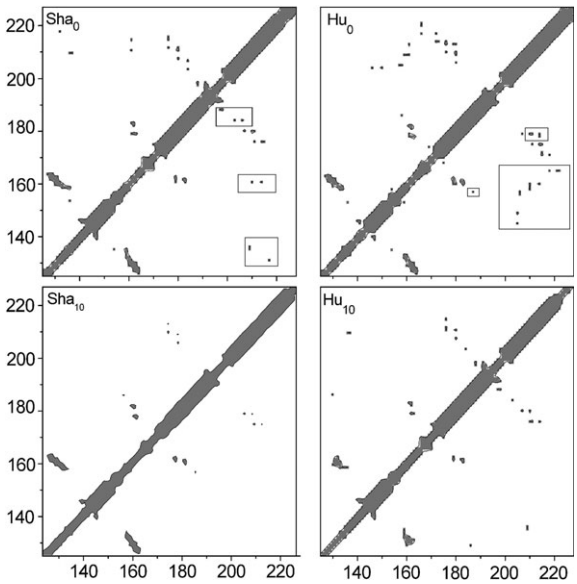

Fig. 4 Residue contact maps of ShaPrP in the native state (Sha_0) and after an elongation of 10 Å (Sha_{10}) and HuPrP in the native state (Hu_0) and after an elongation of 10 Å (Hu_{10}). Two residues were considered to be in contact when the distance between their C(α) atoms was less than 7 Å. Boxes indicate native-like contacts lost after elongation (10%).

Unfolding of TuPrP

Differently from the mammalian prions, it is difficult to ascribe particular molecular events to single peaks of the force–elongation plot relative to the mechanical unfolding of TuPrP (Fig. 2 black line). The unfolding force, even at the maximum elongation explored (100 Å), never exceeds 3500 pN, and the stretching of the protein is reversible up to 30 Å. Contact maps, reported in Fig. 5, calculated for the native state and after an elongation of 10 Å, evidence that in this range some local contacts such as Lys207–Val181, Gln211–Arg178, Cys214–Val177, Gln217–Phe176, Met213–Val161, Val201–Glu146, Val209–Asn140 and Met213–Ser135 are lost. In the range 10–30 Å, the residues that constitute the C-terminal end of helix 3 unfold and move away from the protein core. In the range 30–100 Å, helix 3 unfolds completely. Moreover, differently from the mammalian prions, helix 2 remains folded because of the presence of the loop involving 10 residues (from Lys189 to Thr199), which is stretched before helical unfolding.

Unfolding of ChPrP

When stretched by external forces, ChPrP exhibits a behaviour similar to that observed for TuPrP. In particular, an analysis of frames relative to the early steps of reversible unfolding (extension range 0–10 Å), evidenced that some local contacts, Glu229–Tyr173 and Val222–Arg167, are lost, as shown in Fig. 5. In the range 10–30 Å, the residues that constitute the C-terminal end of helix 3 unfold and move away from helix 2. All these molecular events are reversible. Moreover, in this range, many H-bonds are broken. In particular, the rupture of two of them are evidenced in all simulations: one involves the backbone oxygen of Asn203 and the backbone hydrogen of

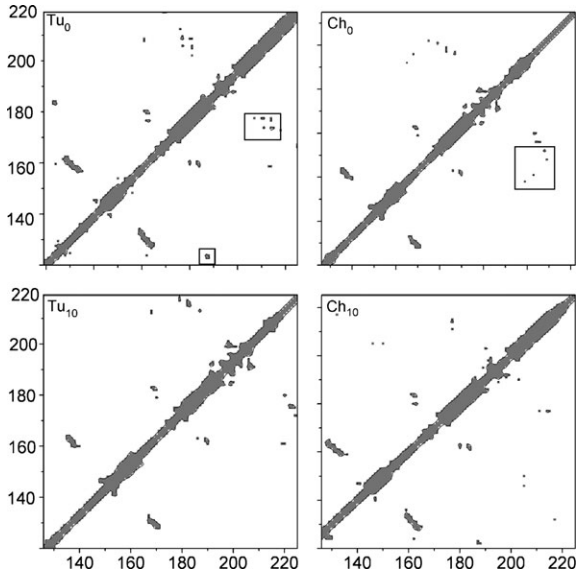

Fig. 5 Residue contact maps of TuPrP in the native state (Tu_0) and after an elongation of 10 Å (Tu_{10}) and of ChPrP in the native state (Ch_0) and after an elongation of 10 Å (Ch_{10}). Two residues were considered to be in contact when the distance between their C(α) atoms was less than 7 Å. Boxes indicate native-like contacts lost after elongation (10%).

Glu206, while the second connects the backbone hydrogen of Asn203 with the backbone oxygen of Pro198. In the range 30–60 Å, the residues belonging to the second part of helix 3 unfold. In addition, the N-terminal loop involving residues from Gly226 to Ser142 begins to extend, but this deformation does not influence the two β-strands involving residues from Val168 to Arg171 and from Tyr135 to Gly138, respectively. In the range 60–100 Å, the residues that constitute the final part of helix 3 unfold completely. The N-terminal loop involving residues from Gly226 to Ser142 continues to extend without any deformation of the two β-strands nearby. Similarly to that found for TuPrP, helix 2 is still folded because of the presence of the loop involving 23 residues (from Glu219 to Ile196), which is stretched before helical unfolding.

Discussion

SMD simulations performed on the globular C-domain of two mammalian and two non-mammalian prion proteins revealed that a higher mechanical force is necessary to unfold mammalian prions and that irreversible events occur earlier with respect to the unfolding of non-mammalian proteins. The irreversible events occurring at the early stages of mammalian prion stretching were ascribed to the loss of effective native-like contacts that are not evident in the structures of the non-mammalian proteins. These contacts mainly involve residues belonging to helices 1 and 3 whose interactions have been found to be important for PrP folding and stability.[12,13] Furthermore, the early steps of mammalian prion unfolding are characterized by the rupture of the H-bonding network connecting the two β-strands of the unstructured N-terminal domain with helix 1. Conversely, in non-mammalian prions the early steps of unfolding are mostly characterized by the

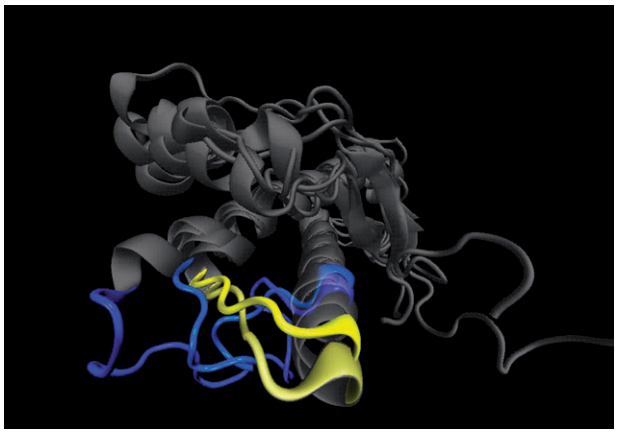

Fig. 6 Superimposed 3D structures of the loops connecting helix 2 with helix 3 in mammalian—HuPrP (light yellow) and ShaPrP (dark yellow)—and non-mammalian—ChPrP (light blue) and TuPrP (dark blue)—prions.

smooth loosening of an elastic loop connecting helix 2 with helix 3 (Fig. 6). Although a quantitative calculation of free energy unfolding profiles from the non-equilibrium force–elongation curves reported here is not possible, the existence of metastable conformers may be deduced from the earlier occurrence of irreversible events along stretching (ruptures of native-like structures) in mammalian prions. Consequently, it may be hypothesized that after the loss of the native-like contacts mammalian prions can explore a number of conformations away from the native state. On the contrary, the mild slope of the stretching forces exhibited by non-mammalian proteins, coupled with the late onset of irreversible events, would allow them to refold more easily after an external perturbation (Fig. 7). While a straightforward extrapolation of these results in a biological context is not simple, the existence of the early steps of protein unfolding of non-native states unable to refold, here observed for mammalian prions, may have important consequences. In fact, the existence of these metastable states may prevent the achievement of the

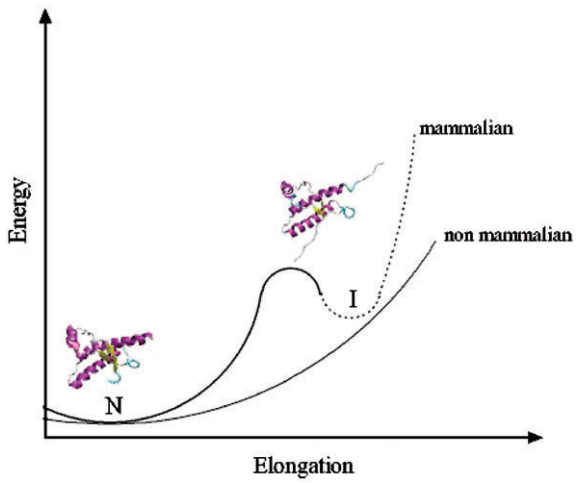

Fig. 7 Schematic drawing of energy *vs.* elongation of mammalian and non-mammalian prions. N and I represent the native and an intermediate state which originate from a reversible (—) and irreversible (···) elongation, respectively.

most stable conformations of proteins and/or lead to the co-existence of many different long-lived conformers. Many authors have proposed that this ''conformational heterogeneity'' may be closely related to the genesis of ''conformational diseases'', because the observed existence of metastable non-native states is believed to boost abnormal pathways of protein misfolding and aggregation.[14–18] It is noteworthy to remind ourselves here that multiple pathways of misfolding have been invoked to explain the difficulties in refolding PrP^{Sc} *in vitro*, the formation of distinct β-sheet-rich abnormal isoforms, the need for a PrP^{Sc} template, and the existence of prion 'strains', *i.e.* clinically distinct disease forms within a single animal species that are not associated with mutations in the PrP gene.[19]

Acknowledgements

This work was financially supported by MIUR (FIRB N° RBNE03PX83, PRIN. 2005035119002). All calculations were performed using the Linux cluster at Cineca high computing center, Casalecchio Di Reno (Bo) Italy.

References

1 S. B. Prusiner, *Science*, 1991, **252**, 1515.
2 F. E. Cohen and S. B. Prusiner, *Annu. Rev. Biochem.*, 1998, **67**, 793.
3 K. M. Pan, M. Baldwin, J. Nguyen, M. Gasset, A. Serban, D. Groth, I. Mehlhorn, Z. W. Huang, R. J. Fletterick, F. E. Cohen and S. B. Prusiner, *Proc. Natl. Acad. Sci. U. S. A.*, 1993, **90**, 10962.
4 A. Horwich and C. Weissman, *Cell (Cambridge, MA, U. S.)*, 1997, **89**, 499.
5 B. Isralewitz, J. Baudry, J. Gullingsrud, D. Kosztin and K. Schulten, *J. Mol. Graphics Modell.*, 2001, **19**, 13.
6 R. Riek, G. Wider, M. Billeter, S. Hornemann, R. Glockshuber and K. Wuthrich, *Proc. Natl. Acad. Sci. U. S. A.*, 1998, **95**, 11667.
7 J. C. Phillips, R. Braun, W. Wang, J. Gumbart, E. Tajkhorshid, E. Villa, C. Chipot, R. D. Skeel, L. Kale and K. Schulten, *J. Comput. Chem.*, 2005, **26**, 1781.
8 H. Liu, S. Farr-Jones, N. B. Ulyanov, M. Llinas, S. Marqusee, D. Groth, F. E. Cohen, S. B. Prusiner and T. James, *Biochemistry*, 1999, **38**, 5362.
9 L. Calzolai, D. A. Lysek, D. R. Perez, P. Guntert and K. Wuthrich, *Proc. Natl. Acad. Sci. U. S. A.*, 2005, **102**, 651.
10 W. L. Jorgensen, J. Chandrasekhar and J. D. Madura, *J. Chem. Phys.*, 1983, **79**, 926.
11 H. Lu and K. Schulten, *Biophys. J.*, 2000, **79**, 51.
12 V. Granata, P. Palladino, B. Tizzano, A. Negro, R. Berisio and A. Zagari, *Biopolymers*, 2006, **82**, 234.
13 L. Ronga, B. Tizzano, P. Palladino, R. Ragone, E. Urso, M. Maffia, M. Ruvo, E. Benedetti and F. Rossi, *Chemical Biology & Drug Design*, 2006, **68**, 139.
14 S. T. Ferreira and F. G. De Felice, *FEBS Lett.*, 2001, **498**, 129.
15 D. Baker and D. A. Agard, *Biochemistry*, 1994, **33**, 7505.
16 A. W. Rietveld and S. T. Ferreira, *Biochemistry*, 1996, **35**, 7743.
17 L. Erijman and G. Weber, *Biochemistry*, 1991, **30**, 1595.
18 A. W. Rietveld and S. T. Ferreira, *Biochemistry*, 1998, **37**, 933.
19 I. V. Baskakov, G. Legname, M. A. Baldwin, S. B. Prusiner and F. E. Cohen, *J. Biol. Chem.*, 2002, **277**, 21140.